



Potentiostatic Start-Up of PEMFCs from Subzero Temperatures

Fangming Jiang* and Chao-Yang Wang**^z

Electrochemical Engine Center (ECEC) and Department of Mechanical and Nuclear Engineering, The Pennsylvania State University, University Park, Pennsylvania 16802, USA

Potentiostatic start-up of a proton exchange membrane fuel cell (PEMFC) from subfreezing temperatures is explored in this work. Taking advantage of hydration of membrane and rising cell temperature, potentiostatic start-up features a drastic increase in current density in the course of a cold start, thus leading to substantially more heat generation and a more rapid cell warmup. It is noted that potentiostatic start-up is more advantageous over its galvanostatic counterpart only when the membrane is dry prior to a cold start with sufficient gas purge. In addition, it is found that lowering the cell thermal mass significantly improves the performance of potentiostatic start-up. Minimizing the heat loss from end plates to the ambient is less critical for start-up processes of short duration. Finally, numerical results indicate that it is possible to achieve a self-start from -30°C in ~ 50 s under realistic conditions using the potentiostatic method. While potentiostatic start-up cannot be used directly for fuel cell stacks, it is a fundamental problem representing innovative current-ramping strategies.

© 2008 The Electrochemical Society. [DOI: 10.1149/1.2927381] All rights reserved.

Manuscript submitted January 31, 2008; revised manuscript received April 7, 2008. Available electronically May 23, 2008.

Quick start-up of a proton exchange membrane fuel cell (PEMFC) engine from subzero temperatures remains a challenge for automotive application. Technical targets of the U.S. Department of Energy for PEMFC stacks in the year 2010 include survivability from -40°C and start-up from -20°C to maximum power in 30 s.¹ While active measures such as external heating may fulfill these targets, studies about PEMFC self-start-up strategies are not only of practical interest, but also of fundamental interest.

Fundamental mechanisms for PEMFC cold start have been clarified by a recent series of experimental and theoretical studies.²⁻¹⁴ That is, water produced from an oxygen reduction reaction (ORR) is removed from the cathode catalyst layer (CL) via absorption into the ionomeric membrane and vapor-phase transport, followed by desublimation in the gas diffusion layer and channels. The remaining water forms ice in the cathode CL. The nature of ice formation in the cathode CL has been investigated by subzero cyclic voltammetry¹³ as well as ex situ cryo-scanning electron microscopy.^{12,14} More detailed discussions on earlier work of cold starts²⁻¹¹ are available in Thomson et al.¹² and Ge and Wang.¹³

Cell temperature plays a pivotal role during subzero start-up of PEMFCs. Rising cell temperature favors the ORR kinetics as well as accelerates water removal from the cathode CL, as both water transport properties in the membrane and vapor-phase diffusion strongly depend on temperature. The fate of a subzero start-up is ultimately determined by the competition between heat generation and ice formation in the cathode CL. A successful start requires the cell to warm up to the freezing point while at the same time keeping ice formation in the cathode CL below the plugging or shutdown threshold. Intricate interactions between ice formation and heat generation occurring in practical cold-start processes have been elaborated recently by Jiang et al.¹⁵

Self-start-up strategies can be roughly classified into two categories: (i) improved water removal approaches to reduce water accumulation, thus lowering ice formation in the cathode CL, and (ii) quick heat generation methods to raise the cell temperature. Some obvious examples of the latter category are lowering the thermal mass of a stack and decreasing heat loss to the ambient. An effective gas purge to minimize residual water in the stack prior to cold start, improved membrane electrode assembly properties to facilitate water transport and storage, and the adjustment of operating parameters that lead to delayed ice formation in the CL all belong to the former category.

The total heat generation rate ($\text{J}/\text{cm}^2/\text{s}$) during a start-up process is roughly proportional to the current density such that

$$\dot{Q}_{\text{total}} \approx (E_{\text{h}} - U_{\text{cell}})I \quad [1]$$

where E_{h} denotes the thermal potential of $\text{H}_2\text{-O}_2$ reaction, with the product water being ice. During a potentiostatic start-up (with cell voltage U_{cell} fixed), the discharging current density (I) varies strongly with the hydration of the membrane. Typically, the current density is low in the early stages of start-up, which produces water for the hydration of the membrane. Subsequently, the current density increases with membrane hydration, creating more heat to warm up the cell as evident from Eq. 1. The rapid temperature rise, in turn, facilitates water transport from the cathode CL to the membrane, resulting in faster membrane hydration and hence further increased current density. This nonlinear feedback among membrane hydration, current ramping, and cell temperature rise makes potentiostatic start-up intrinsically an ideal strategy for PEMFC cold start. In contrast, galvanostatic start-up does not take advantage of the nonlinear feedback explicitly expressed in Eq. 1, as the current density remains independent of membrane hydration and the voltage variation is relatively small. Thus, heat generation does not increase appreciably, as can be seen from Eq. 1.

While potentiostatic start-up is not directly applicable to fuel cell stacks, it is used in the present work as a surrogate to illustrate the fundamentals of a large class of current-ramping start-up strategies applicable to fuel cell stacks. Our objective is to delineate the basic characteristics of heat generation and ice formation in potentiostatic start-up as compared to the more commonly studied galvanostatic start-up. Selective case studies are carried out to elucidate the fundamental characteristics of potentiostatic start-up, its advantages, and the conditions under which it is more advantageous. Results herein are useful to guide the design of rapid self-cold-start strategies in practice.

The present paper is organized as follows. The next section briefly introduces a non-isothermal, multiphase cold-start model developed by Mao et al.⁸ and Jiang et al.,¹⁵ which is used as a tool to analyze the non-isothermal, potentiostatic start-up of interest in this work. The third section presents detailed results in three subsections. First, comparisons between potentiostatic and galvanostatic cold start are made to delineate the fundamental characteristics of potentiostatic start-up. Second, advantages of potentiostatic start-up are illustrated through a series of parametric studies. Third, an example of current-ramping start-up is given to demonstrate the application of quasi-potentiostatic start-up in practice. Conclusions are summarized in the final section.

Cold-Start Model

The model used in this work is a continuation of Jiang et al.¹⁵ This non-isothermal, multiphase model fully accounts for the transient transport and electrochemical processes with ice formation,

* Electrochemical Society Student Member.

** Electrochemical Society Active Member.

^z E-mail: cwx31@psu.edu

Table I. Baseline parameters.

Quantity	Value
Ambient start-up temperature, T_0	-20 or -30°C
Initial ice fraction in CL	0
Current density in galvanostatic start-up, I	100 mA/cm ²
Thermal mass of the cell, $(mC_p)_{\text{cell}}^a$	0.5 J/cm ² K
Heat convection coefficient, h^a	40 W/m ² K
Initial water content in MEA, λ_i^a	3.0
Cell voltage in potentiostatic start-up, U_{cell}^a	0.66 V (-20°C start-up) or 0.61 V (-30°C start-up)

^a Default value.

and can be concisely summarized in the form of the following governing equations^{8,15}

Continuity equation

$$\frac{\partial(\varepsilon_s \rho_s)}{\partial t} + \frac{\partial(\varepsilon \rho)}{\partial t} + \nabla \cdot (\rho \mathbf{u}) = 0 \quad [2]$$

Momentum conservation

$$\frac{\partial(\rho \mathbf{u} / \varepsilon)}{\partial t} + \nabla \cdot \left(\frac{\rho \mathbf{u} \mathbf{u}}{\varepsilon^2} \right) = \nabla \cdot (\mu \nabla \mathbf{u}) - \nabla P + S_u \quad [3]$$

Species conservation

$$\frac{\partial(\varepsilon C^i)}{\partial t} + \nabla \cdot (\mathbf{u} C^i) = \nabla \times (D_{\text{eff}}^i \nabla C^i) + S_C^i \quad [4]$$

Charge conservation (electrons)

$$0 = \nabla \cdot (\sigma_s^{\text{eff}} \nabla \phi_s) + S_{\phi_s} \quad [5]$$

Charge conservation (protons)

$$0 = \nabla \cdot (\kappa_e^{\text{eff}} \nabla \phi_e) + S_{\phi_e} \quad [6]$$

Details of the non-isothermal, multiphase model were presented by Jiang et al.¹⁵ and hence are not repeated here. One additional assumption invoked in the present work is that the whole fuel cell is treated as a lumped thermal system with a spatially uniform temperature. Therefore, the energy equation is simplified as shown shortly and then coupled with the above partial differential equation system. Geometrical parameters and electrochemical, physical, and transport properties are the same as used in Jiang et al.,¹⁵ except for the parameters tabulated in Table I. For more details on this model, one may refer to the works by Jiang et al.¹⁵ and Mao et al.⁸

Lumped thermal model.— In a single cell, the temperature variation between the CL and current collector is negligibly small under small to medium current densities commonly used in cold start. Substantial temperature variation along the flow direction may exist, depending on the initial water distribution prior to cold start.¹⁵ This is because the initial water distribution dictates the current density distribution and hence the heat generation distribution, which can lead to a temperature difference greater than 10°C along the flow direction.¹⁵ In this work, however, we assume that the cell is prepared with an equilibrium purge,⁷ resulting in a uniform initial membrane water content. The assumption thus justifies the existence of a uniform temperature throughout the cell and hence the use of a lumped thermal model.

In the lumped thermal model, the total heat generation rate during cold start is simply the volumetric integration of all local heat sources, such that

$$\begin{aligned} \dot{Q}_{\text{total}} = & \frac{1}{A} \int_{V, \text{CLs}} \left[j \left(\eta + T \frac{dU_0}{dT} \right) + \frac{i_e^2}{\kappa_e} + \frac{i_s^2}{\sigma_s^{\text{eff}}} + \dot{q}_{\text{H}_2\text{O}} h_{\text{gs}} \right] dV \\ & + \frac{1}{A} \int_{V, \text{mem}} \frac{i_e^2}{\kappa_e} dV \end{aligned} \quad [7]$$

Heat losses from the cell to the surroundings include two contributions: (i) heat loss brought out by exhaust gases, and (ii) convective heat loss from outer surfaces of the cell's bipolar plates. Mathematically, this can be expressed as

$$\dot{Q}_{\text{loss}} = \frac{1}{A} [(mC_p)_{\text{out}} T - (mC_p)_{\text{in}} T_0] + h(T - T_0) \quad [8]$$

where h is the heat convection coefficient on the cell outer surfaces. Applying energy balance to the cell and invoking the assumption of spatially uniform temperature, the cell temperature can be calculated from

$$(mC_p)_{\text{cell}}(T - T_0) = \int_0^t (\dot{Q}_{\text{total}} - \dot{Q}_{\text{loss}}) dt \quad [9]$$

where the cell thermal mass, $(mC_p)_{\text{cell}}$, has a unit of J/m² K, which is the volumetric summation of heat capacities of individual components divided by the electrode active area. The uniform cell temperature solved by Eq. 9 is fully coupled to other conservation equations with the assumption of instantaneous ice formation. While the temperature is spatially uniform, the ice formation rate is location-dependent as both water production and removal rates vary spatially as to be determined from Eq. 3-6.

Numerical details of solving Eq. 3-6 in conjunction with Eq. 9 can be found in the works of Mao et al.⁸ and Jiang et al.¹⁵ Both potentiostatic and galvanostatic start-up can be simulated by the same computer model with the only difference in the boundary condition for the electronic potential, i.e., constant voltage in potentiostatic start-up but constant current density in galvanostatic start-up. These non-isothermal, multiphase, transient simulations can be run routinely on a single personal computer, as evident from the extensive parametric studies presented below.

Results and Discussion

The goals of the present work are to reveal the interactions of ice formation and heat generation during potentiostatic start-up and to provide useful information for the design of optimal start-up strategies using current ramping. Therefore, detailed spatial distributions of the ice fraction, current density, and membrane water content are not the main focus of this work. Rather, evolution of the average cell temperature and ice fraction at the center of the cathode CL is to be presented to elucidate a quantitative relationship between ice formation and heat generation.

Potentiostatic vs galvanostatic start-up.— To examine the fundamental features of cold-start processes involving current ramping, potentiostatic start-up is compared to the more commonly used galvanostatic start-up. We compare potentiostatic and galvanostatic start-up under the condition that the initial power output and hence the initial heat generation are kept the same. This requires that the constant cell voltage in the potentiostatic start-up is exactly equal to the initial voltage resulting from the comparative galvanostatic start-up. On this basis, all initial conditions, i.e., current density, voltage, temperature, and water distribution, remain identical in potentiostatic and galvanostatic start-up.

A PEMFC started from -20°C is considered first. Potentiostatic start-up is under a fixed voltage of 0.66 V, while galvanostatic start-up has a constant current density of 100 mA/cm². Upon start-up, both potentiostatic and galvanostatic operations produce the same power density of 0.66 V × 100 mA/cm². Figure 1 displays the evolution of cell voltage during galvanostatic start-up and current density during potentiostatic start-up. Initially, the membrane is

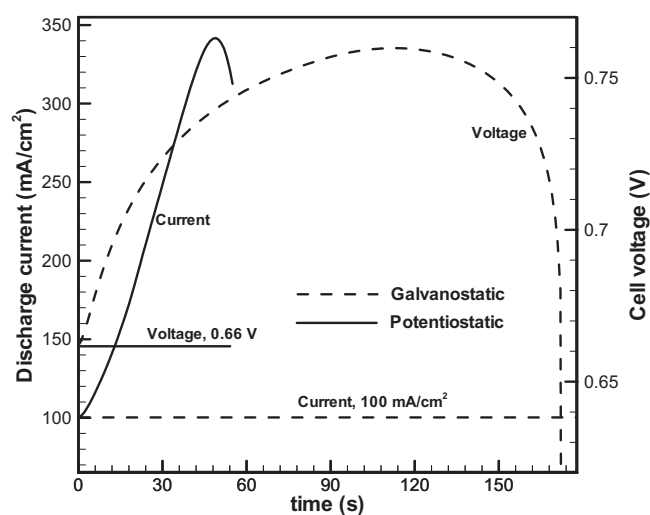


Figure 1. Evolution of cell voltage and current density during cold start from -20°C .

dry ($\lambda_i = 3.0$), resulting in a very high ohmic resistance. After start-up, the membrane and ionomer in CLs are gradually hydrated by water produced from an ORR, lowering the protonic resistance. Both the cell voltage during galvanostatic start-up and the current density during potentiostatic start-up are seen to increase. Once the water vapor concentration inside the cathode CL reaches saturation, ice begins to precipitate. Solid ice then blocks the pathways for oxygen transport and reduces the electrochemical active area, leading to deteriorated cell operation; consequently, the cell voltage in galvanostatic start-up begins to drop at ~ 113 s into start-up, while the current density in potentiostatic start-up begins to drop at ~ 49 s into start-up. When the ice fraction in the cathode CL approaches unity, cell operation ceases. The galvanostatic start-up is seen to shut down at ~ 173 s, while for the potentiostatic start-up, at 55 s into start-up, the cell temperature already rises to 0°C , indicating a successful self-start. More discussion on the cell temperature evolution during potentiostatic start-up is given below in relation to Fig. 4.

As can be seen from Fig. 1, the current density in potentiostatic start-up varies greatly, from 100 to ~ 340 mA/cm^2 in a short period of 49 s. As indicated by Eq. 1, the heat generation rate is linearly dependent on the current density. It can thus be concluded that heat generation in potentiostatic start-up increases much faster than in galvanostatic start-up. This is a prime advantage of potentiostatic operation for cold start. Figure 2 compares the total heat generation rate between the two cold-start operations. At the instant of loading, the potentiostatic and galvanostatic start-up yields exactly the same amount of waste heat. In the galvanostatic start-up, the total heat generation rate slightly decreases in the early stage (from 0 to ~ 90 s) due to the gradual increase of cell voltage (see Fig. 1), then follows a slight increase due to ice formation after ~ 90 s and the diminishing cell voltage from ~ 113 s. In the potentiostatic start-up, the total heat generation rate keeps increasing from the beginning of cold start until the ice formation effect prevails (at ~ 49 s), after which the decrease in current density makes the total heat generation decrease. At ~ 22 s into potentiostatic start-up, ice begins to form, and latent heat released further differentiates the two heat generation curves. Overall, the total heat generation rate in the potentiostatic start-up rises as high as 0.32 W/cm^2 , while that in the galvanostatic start-up remains below 0.09 W/cm^2 throughout the operation. The area underneath each heat generation curve represents the total heat produced, which directly dictates the final cell temperature. As seen from Fig. 2, it is apparent that the heat generation from potentiostatic start-up is much more than that in galvanostatic start-up.

Water flow at subzero temperatures plays a controlling role in cold start. Jiang et al.¹⁵ analyzed water flow in detail, separating

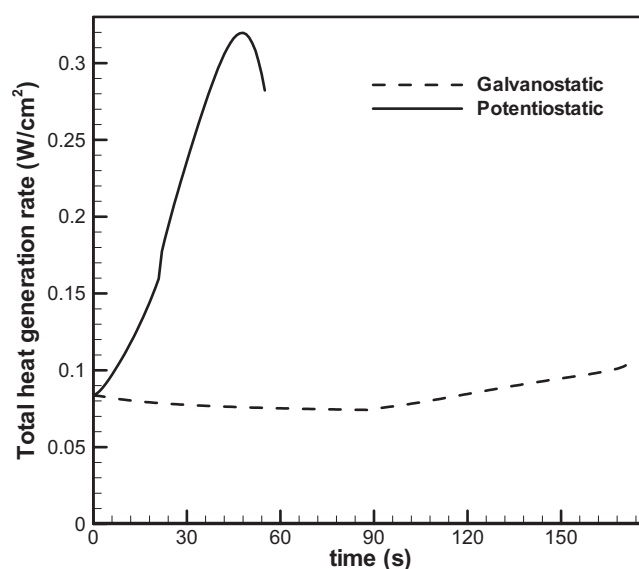


Figure 2. Comparison of total heat generation rates during galvanostatic and potentiostatic start-up from -20°C .

water production/transport and ice formation on the cathode side of a fuel cell. An overall water balance can be expressed as¹⁵

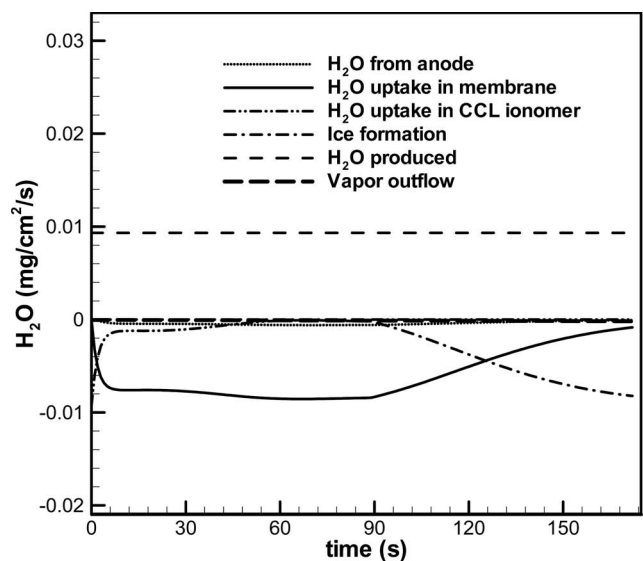
$$\dot{n}_{\text{pro}} + \dot{n}_{\text{CCL}} + \dot{n}_{\text{mem}} + \dot{n}_{\text{anode}} + \dot{n}_{\text{ice}} + \dot{n}_{\text{outflow}} = 0 \quad [10]$$

where \dot{n}_{pro} , \dot{n}_{outflow} , \dot{n}_{CCL} , \dot{n}_{mem} , \dot{n}_{anode} , and \dot{n}_{ice} represent the water production rate, vapor outflow rate, water uptake rate in the ionomer of cathode CL, water uptake rate in the membrane, water transport rate from the anode side, and ice formation rate in the cathode CL, respectively. The sign convention here is such that \dot{n}_{pro} is positive, while \dot{n}_{CCL} , \dot{n}_{ice} , and \dot{n}_{outflow} are negative as they take away the product water. In the membrane (or anode), if water back-diffusion dominates the water content variation, \dot{n}_{mem} (or \dot{n}_{anode}) takes a negative value, otherwise a positive value.

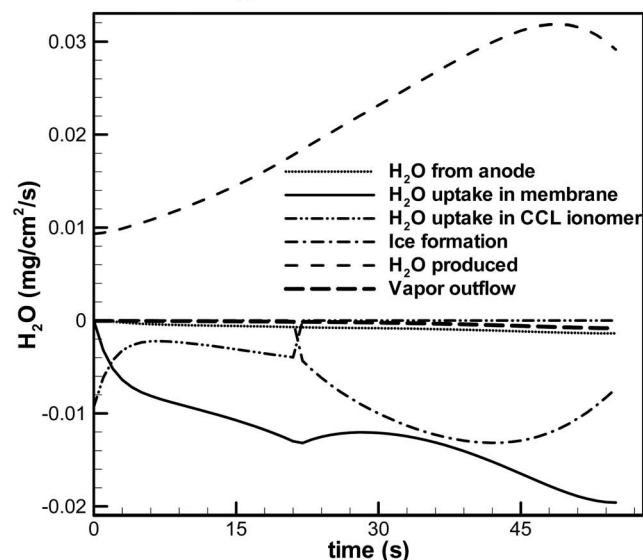
The water flow analysis for both potentiostatic and galvanostatic start-up (from -20°C) has been carried out and compared in Fig. 3. In general, the water production rate in potentiostatic start-up is much higher, as are the membrane water uptake and ice formation rates. For both potentiostatic and galvanostatic start-up, the removal of product water from the CL primarily depends on water diffusion into the membrane, whereas vapor outflow makes only a negligible contribution. Water uptake by the initially dry ionomer in the cathode CL is significant only in the early stage, at 0–48 s for the galvanostatic start-up and at 0–22 s for the potentiostatic start-up. After the ionomer in the cathode CL is fully hydrated, the balance of water between production and transport forms ice in the cathode CL. Ice begins to form at ~ 90 s into the galvanostatic start-up, in contrast to ~ 22 s into the potentiostatic start-up.

The water production rate ($=M^{\text{H}_2\text{O}}/2F$ theoretically) is directly proportional to the current density. It is seen from Fig. 3 that the water production rate is ~ 0.0093 $\text{mg}/\text{cm}^2/\text{s}$ in the galvanostatic start-up, while it varies between 0.0093 and 0.032 $\text{mg}/\text{cm}^2/\text{s}$ in the potentiostatic start-up due to the increasing current density (see Fig. 1). A faster water production rate and more rapid cell temperature rise (due to more heat generation; see Fig. 2) accelerate the hydration of the membrane during potentiostatic start-up, quickly lowering the ohmic resistance and hence increasing the current density, which in turn results in a further increase in heat generation. This nonlinear feedback eventually leads to a successful quick self-start.

Figure 4 compares the evolution of the ice fraction in the center of the cathode CL, and the evolution of cell temperature between potentiostatic and galvanostatic start-up. For the galvanostatic start-up, due to the low current density (100 mA/cm^2), ice formation is slow and the cell operation time is extended. However, low current



(a)



(b)

Figure 3. Water flow during cold start from -20°C : (a) galvanostatic and (b) potentiostatic.

density operation only creates low heat generation, resulting in a slow temperature rise. When the ice fraction in the cathode CL reaches unity, the cell temperature has risen only to $\sim -4^{\circ}\text{C}$, signifying a failed cold start. In contrast, the potentiostatic start-up creates a much more rapid cell temperature rise due to the dramatically increasing current density (see Fig. 1). In spite of the much faster ice formation, the cell temperature rises to 0°C while the ice fraction in cathode CL remains below unity, signifying a successful self-start. Note that both temperature evolution curves in Fig. 4 begin with the same slope, as it is indicative of the same heat generation rate at $t = 0$ in potentiostatic and galvanostatic start-up.

Clearly, the main reason that potentiostatic start-up is more advantageous over galvanostatic start-up is that the former entails a higher heat generation. Integrated over the entire fuel cell, various heat generation rates, along with various heat loss rates calculated from Eq. 7, are shown as a function of time in Fig. 5. Once again, at $t = 0$ the potentiostatic start-up produces the same amount of heat generation/loss as the galvanostatic start-up. As the irreversible re-

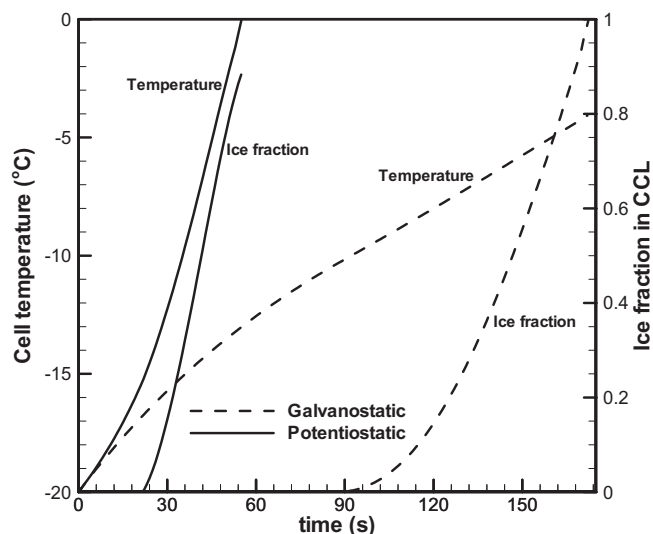


Figure 4. Comparison of ice fraction and cell temperature evolution during galvanostatic and potentiostatic start-up from -20°C .

action heat and entropic heat are both linearly dependent on the current density, they increase rapidly with time during potentiostatic start-up and quickly exceed their counterparts in galvanostatic start-up. For the galvanostatic start-up, the lowering of the protonic resistance results in a gradual decline in ohmic (Joule) heat, while the ohmic heat in the potentiostatic start-up is more controlled by the increasing current density; it slightly increases until the current density begins to drop at ~ 49 s. In addition, the faster ice formation in potentiostatic start-up releases more latent heat, further deviating the total heat generation of the two cases.

Various heat losses are plotted as negative values in Fig. 5. With a constant ambient temperature, the heat loss rate from the end plates is linearly dependent on the cell temperature. The potentiostatic start-up has a faster heat loss due to the more quickly rising cell temperature. When the cell temperature approaches 0°C , the heat loss (~ 0.08 W/cm²) consumes about 26% of the total heat generation (~ 0.3 W/cm²). This indicates that suppressing convective heat loss from bipolar plates is beneficial to cold start. Due to the relatively small reactant flow stoichiometry (e.g., 2.0), the heat brought out by exhaust gases is negligibly small in both cold-start cases. Although the convective heat loss rate in potentiostatic start-up is higher than that in galvanostatic start-up, the accumulated heat loss in the former is lower due to a much shorter duration. Therefore, more heat is available for cell warmup in potentiostatic start-up. Generally speaking, rapid cold start is less adversely affected by heat loss to the surroundings.

Another simulation of the PEMFC cell starting from -30°C was conducted. The galvanostatic start-up had a constant current density, still 100 mA/cm². As the ohmic resistance was larger at the lower temperature, the cell voltage during potentiostatic start-up was now fixed at 0.61 V to ensure the same power density of 0.61 V \times 100 mA/cm² at the beginning of start-up. Figure 6 displays the evolution of the cell voltage during galvanostatic start-up and current density during potentiostatic start-up. The cell voltage in galvanostatic start-up and the current density in potentiostatic start-up both feature a rise period due to the gradual hydration of the initially dry membrane, followed by a continual decrease or even quick dropdown as a result of ice formation. Eventually, both cold-start operations are shut down. A difference, however, is that the cell shutdown in potentiostatic start-up occurs at ~ 50 s, as compared to ~ 135 s in galvanostatic start-up.

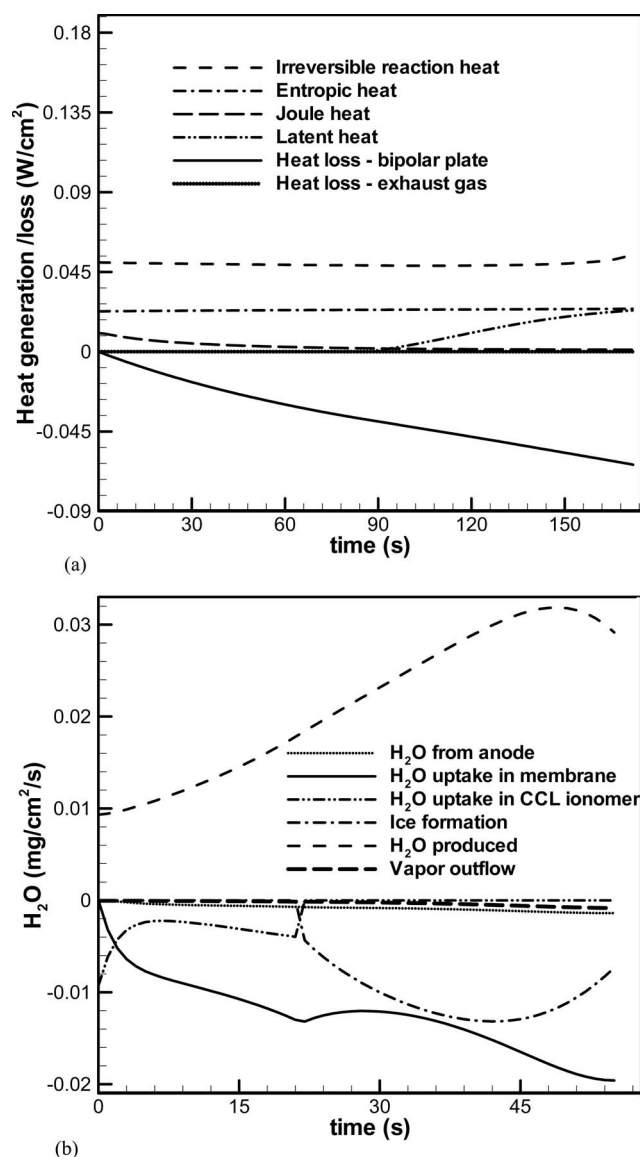


Figure 5. Evolution of various heat generations (+)/losses (-) during cold start from -20°C : (a) galvanostatic and (b) potentiostatic.

Figure 7 compares the evolution of the ice fraction in the cathode CL and cell temperature during the two -30°C cold-start operations. In both cases, the ice fraction in the cathode CL reaches unity while the cell temperature is still below 0°C , signifying a failed cold start. For the potentiostatic start-up, the cell temperature quickly rises to $\sim -14^{\circ}\text{C}$ before the cold-start operation shuts down by ice formation. Although the galvanostatic start-up can operate for a long time, the cell temperature can only be elevated to $\sim -15^{\circ}\text{C}$.

For a cell operating at a lower temperature, the membrane water uptake becomes more sluggish and proton transport experiences a higher resistance. The potential of the current density increase during potentiostatic start-up thus diminishes, thereby decelerating the increase of the heat generation rate. Moreover, a lower ambient start-up temperature requires more energy to bring the cell temperature to 0°C . These two factors combine to result in a failure of the potentiostatic start-up from -30°C . For the galvanostatic start-up from -30°C , the low current density operation does not even have a chance to warm up the cell to 0°C , because the heat loss from the end plates consumes all the heat generation when the cell temperature approaches 0°C (refer to Fig. 5b).

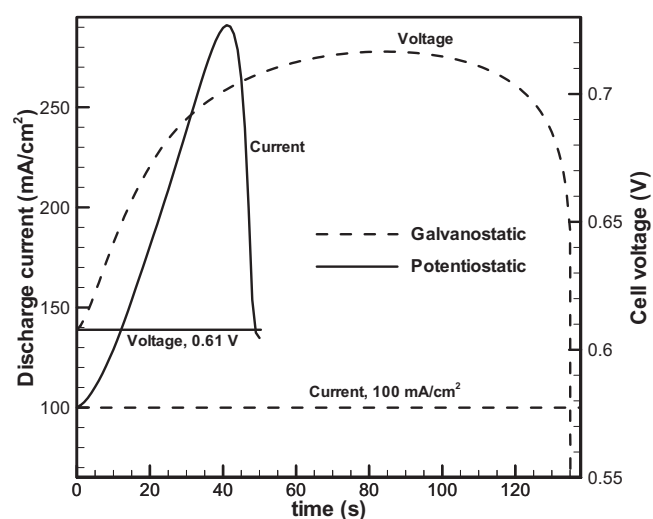


Figure 6. Evolution of cell voltage and current density during cold start from -30°C .

Parametric studies.— Effects of cell thermal mass, convective heat loss (from bipolar plates to the ambient), initial membrane water content, and cell voltage on the performance of potentiostatic start-up are explored. In this section, only potentiostatic start-up from -30°C is considered, and cell voltage is set at 0.61 V unless explicitly stated otherwise.

Cell thermal mass is defined as the volumetric average of heat capacitances of all cell components. Bipolar plates contribute to the majority of cell thermal mass. Assuming graphite bipolar plates as the baseline in the present work, the cell thermal mass is calculated to be $0.5 \text{ J/cm}^2/\text{K}$. Other values of cell thermal mass, 0.4, 0.3, and $0.2 \text{ J/cm}^2/\text{K}$, respectively, are numerically simulated. Figure 8 displays the evolution of current density during start-up for fuel cells of different thermal mass. Cell thermal mass directly determines the amount of thermal energy needed for a cell to warm up to 0°C . As expected, the effect of cell thermal mass on the performance of potentiostatic start-up is very significant. For the cell of the smallest thermal mass, $0.2 \text{ J/cm}^2/\text{K}$, the current density quickly increases as high as $\sim 550 \text{ mA/cm}^2$, and the large quantity of heat generated leads to a successful self-start in as little as $\sim 30 \text{ s}$. For the other

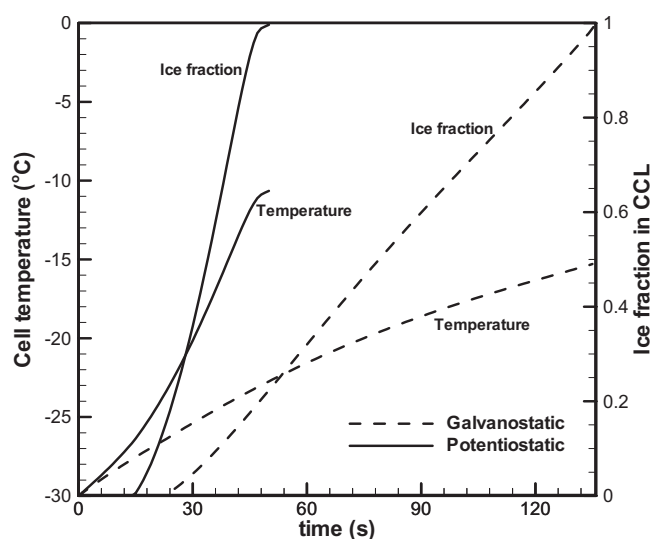


Figure 7. Comparison of ice fraction and cell temperature evolution during galvanostatic and potentiostatic start-up from -30°C .

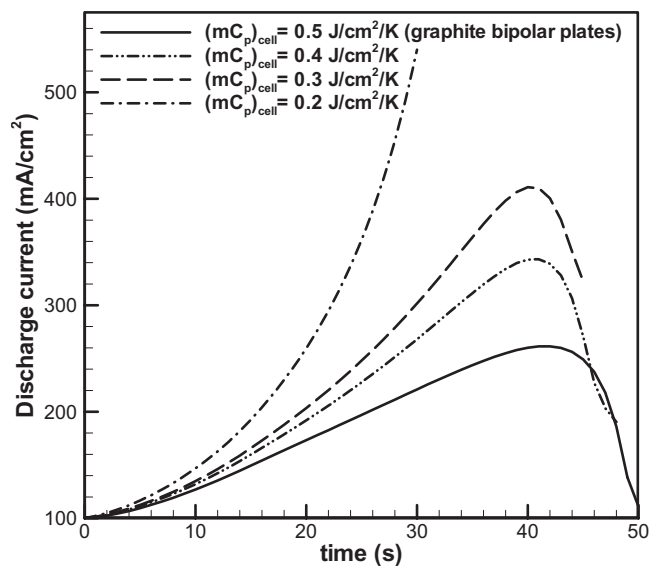
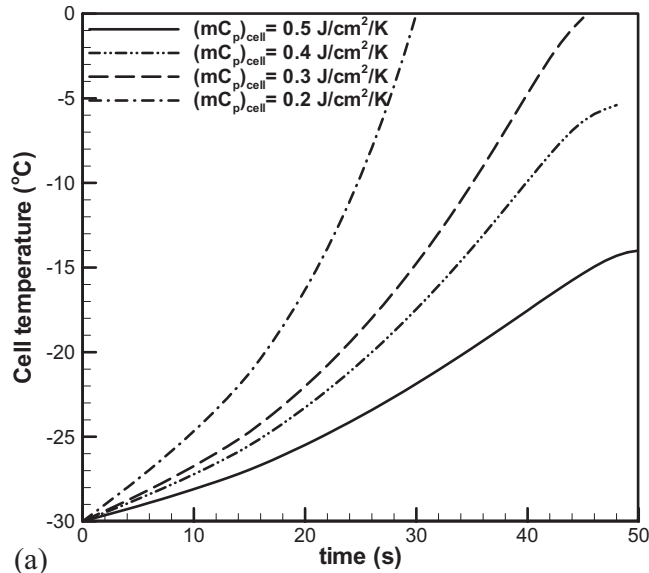
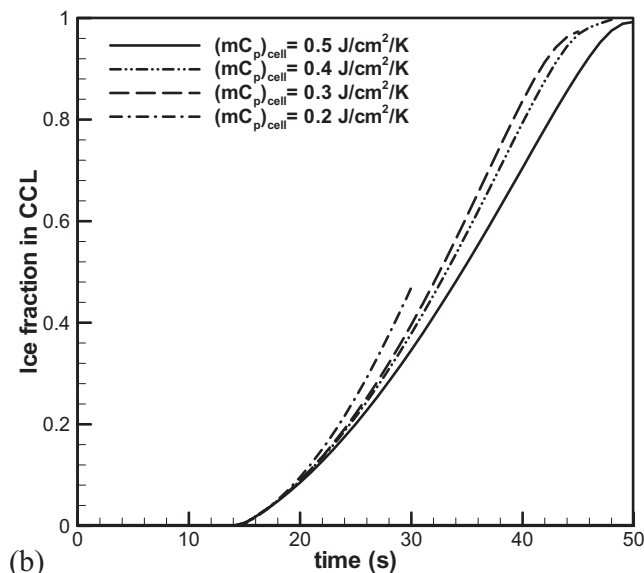


Figure 8. Evolution of current density during potentiostatic start-up from -30°C with various cell thermal mass.



(a)



(b)

Figure 9. Evolution of (a) temperature and (b) ice fraction in the cathode CL during potentiostatic start-up from -30°C with various cell thermal mass.

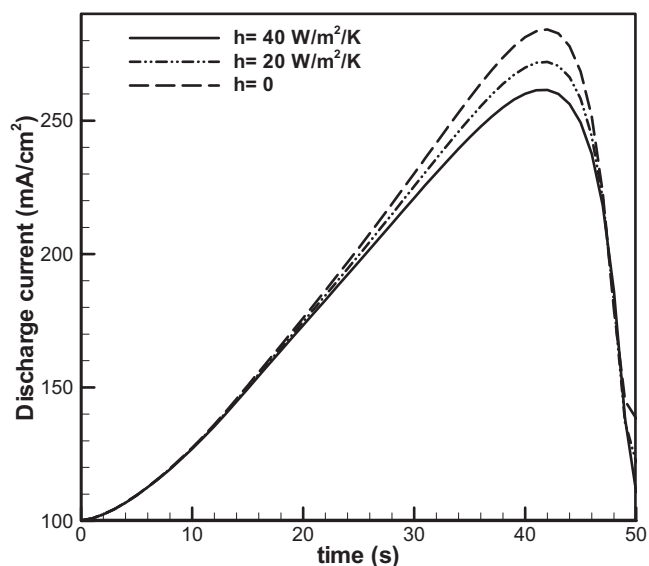


Figure 10. Effect of convective heat loss (from bipolar plates to the ambient) on current density evolution during potentiostatic start-up from -30°C .

three cases with a larger thermal mass, the current densities during start-up increase in an early period of long duration, then quickly decrease. From the temperature and ice fraction evolution as shown in Fig. 9, the start-up operations with cell thermal mass of 0.5 and 0.4 $\text{J}/\text{cm}^2/\text{K}$ shut down, while that with a cell thermal mass of 0.3 $\text{J}/\text{cm}^2/\text{K}$ or lower succeeds as the cell temperature is elevated to 0°C before the ice formed fills the cathode CL. The impact of cell thermal mass on ice formation in the CL is shown in Fig. 9b. It is seen that, for the cold start with cell thermal mass of 0.2 $\text{J}/\text{cm}^2/\text{K}$, the ice fraction in cathode CL stays as low as ~ 0.5 when the cell temperature reaches 0°C , signifying a rapid start.

Heat losses from a cell or stack consume the heat generated during cold start, thereby reducing the heat used to warm up the cell. A major mechanism of heat loss is thermal convection from the end plates to the ambient. By changing the heat convection coefficient h , the effect of heat loss on cold-start performance is numerically studied. The evolution curves of current density for various h are displayed in Fig. 10 and the evolution curves of cell temperature and ice fraction are shown in Fig. 11. The current density exhibits a

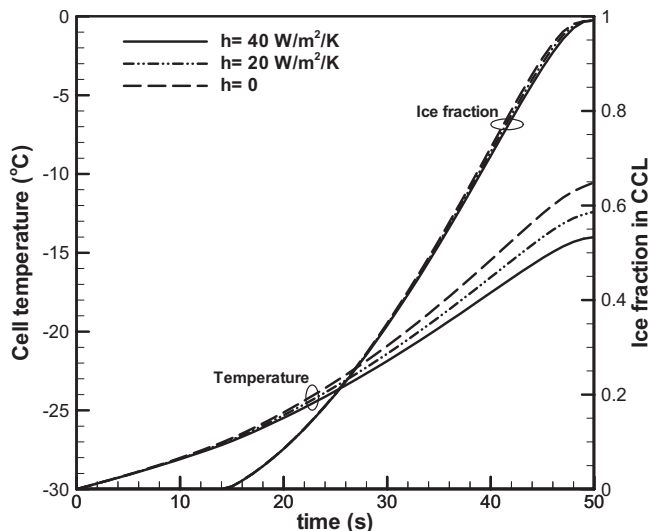


Figure 11. Effect of convective heat loss on temperature and ice fraction evolution during potentiostatic start-up from -30°C .

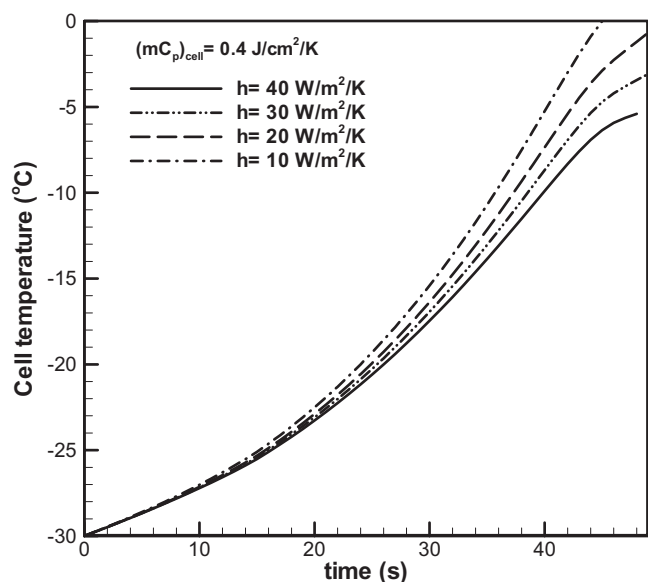


Figure 12. Effect of convective heat loss on cell temperature evolution during potentiostatic start-up from -30°C with the cell thermal mass of $0.4 \text{ J/cm}^2/\text{K}$.

higher peak in potentiostatic start-up and the cell is also warmed up to a higher temperature if h is smaller. There is relatively little difference between the ice fraction curves for different h values. All three cases undergo shutdown as the ice fraction in cathode CL grows to unity at $\sim 50 \text{ s}$ into start-up. Comparing the two cases of $h = 40 \text{ W/m}^2/\text{K}$ and $h = 0$ (adiabatic) shows that the latter can bring the cell temperature to $\sim -10^{\circ}\text{C}$, while the former reaches $\sim -14^{\circ}\text{C}$. Here, the heat loss during $h = 40 \text{ W/m}^2/\text{K}$ start-up is estimated to be $\sim 20\%$ of the total heat generation. Controlling this amount of heat loss is not sufficient to change the fate of start-up under the conditions considered. However, if the cell thermal mass is smaller, say $0.4 \text{ J/cm}^2/\text{K}$, minimizing this heat loss can significantly affect cold-start performance, as shown in Fig. 12.

Figure 12 displays the temperature evolution during four cold-start operations from -30°C with various heat convection coefficients. The cell thermal mass is reduced to $0.4 \text{ J/cm}^2/\text{K}$, and thus the cell is easier to warm up. Lowering h down to $10 \text{ W/m}^2/\text{K}$

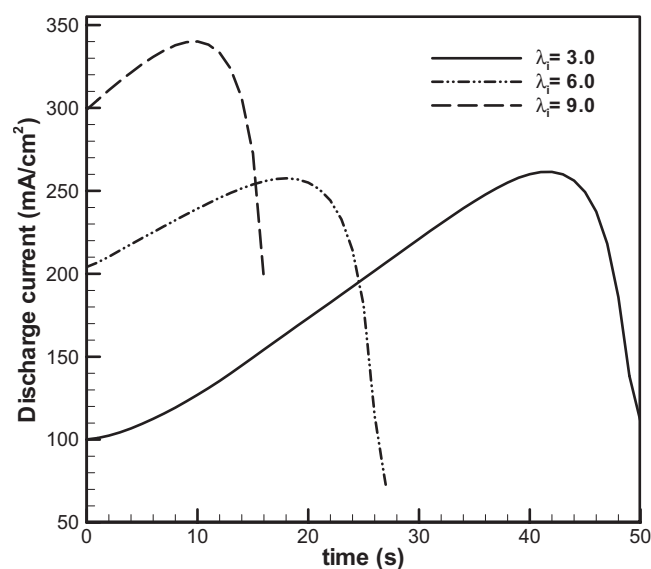


Figure 13. Evolution of current density during potentiostatic start-up ($U_{\text{cell}} = 0.61 \text{ V}$) from -30°C with various initial membrane water content.

allows the cell temperature to rise to 0°C before ice completely fills the cathode CL, signifying a successful start. In these cases, reducing the convective heat loss becomes instrumental to improved cold-start performance.

The initial water content in the membrane dictates the extent of membrane water uptake, and hence has a significant effect on cold-start performance.⁶⁻⁹ Figure 13 compares the current density evolution from three potentiostatic start-up operations with initial membrane water content of 3, 6, and 9 mol H_2O per mol SO_3^- , respectively. A wetter membrane facilitates proton transport, and thus the cell produces a higher current density. All the current density curves increase in the early stage of cell operation, and then quickly drop. The current density in the start-up operation with an initially drier membrane exhibits a longer rising period and higher rising amplitude. Temperature and ice fraction evolution curves are depicted in Fig. 14. All three cold-start operations shut down as the ice fraction in the cathode CL reaches unity while cell temperature is still far below 0°C . Cold-start operation with an initially wetter membrane shuts down more quickly due to the higher current den-

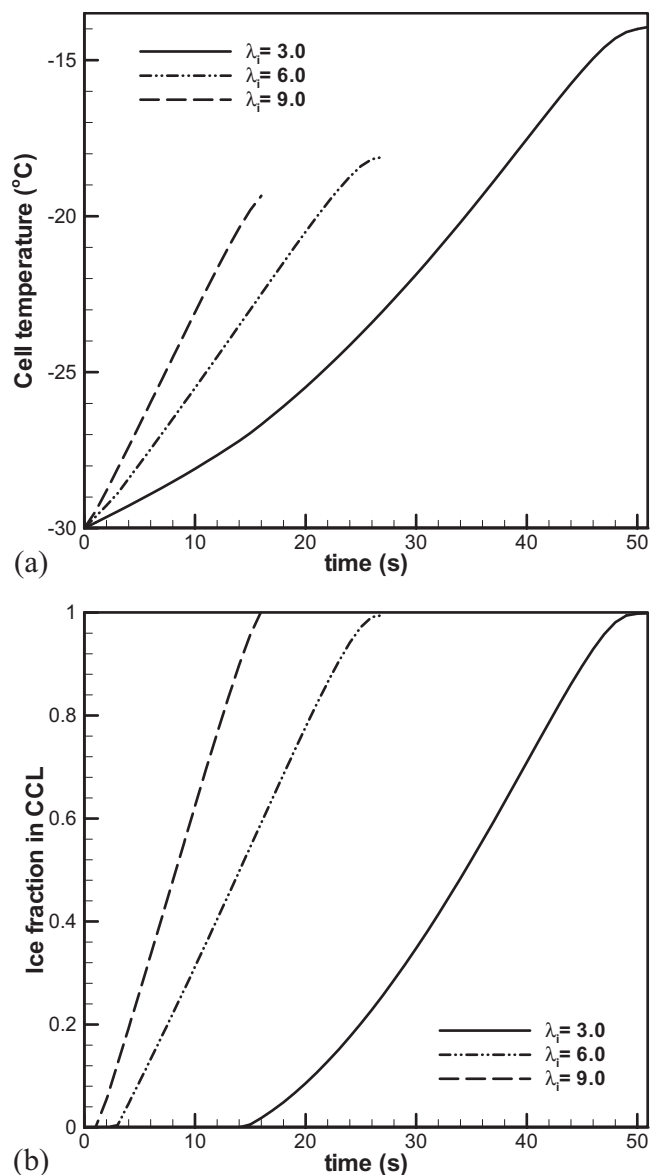


Figure 14. Evolution of (a) temperature and (b) ice fraction in the cathode CL during potentiostatic start-up from -30°C ($U_{\text{cell}} = 0.61 \text{ V}$) with various initial membrane water content.

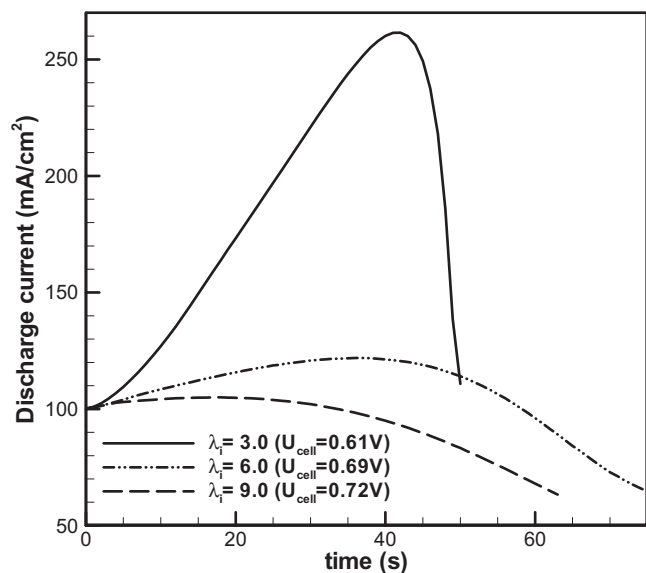


Figure 15. Comparison of current density evolution of potentiostatic start-up from -30°C with various initial membrane water content.

sity and diminished membrane water storage potential. A successful potentiostatic start critically requires an ionomeric membrane with sufficient water storage capacity.

As shown in Fig. 13, the three cold-start operations begin with different current density due to the different initial membrane water content when the same constant cell voltage (0.61 V) is applied. Additionally, three potentiostatic start-up operations, which have different initial membrane water content of 3, 6, and 9, respectively, and also different start-up voltage of 0.61, 0.69, and 0.72 V, respectively, are simulated. The different cell voltages are chosen to match the resulting current density at $t = 0$, maintaining 100 mA/cm^2 in all three cases. Figure 15 compares the current density evolution of these three cold-start operations. The wetter membranes become fully hydrated shortly into start-up, and thus the current density in the corresponding cold-start operations increases only slightly, followed by a decline once the ice formation in the CL becomes significant. In contrast, the drier membrane case exhibits a strong rise

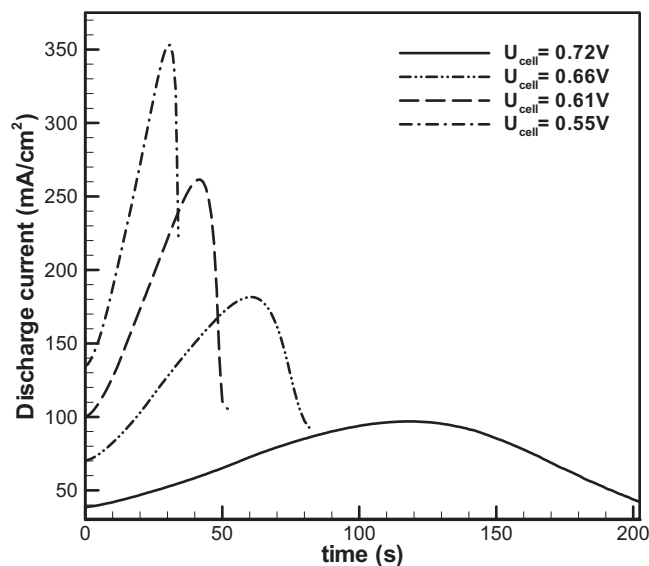


Figure 16. Evolution of current density during potentiostatic start-up from -30°C with various cell voltages.

in current density characteristic of potentiostatic start-up. Therefore, an initially dry membrane is necessary for the potentiostatic mode to succeed.

Finally, the effect of cell voltage on the performance of potentiostatic start-up was explored. Figure 16 displays the current density evolution during potentiostatic start-up operations with various discharge voltage. A change of cell voltage does not affect the overall variation trend of current density, increasing first and then decreasing with time. A higher cell voltage simply leads to a low current density operation and also a long duration of operation.

Evolution curves of temperature and ice fraction during potentiostatic start-up operations of various cell voltage are shown in Fig. 17. Potentiostatic start-up of higher voltage does not favor the cell temperature rise due primarily to the lower current density and the longer time of exposure to the subfreezing ambient (more heat loss). The cell temperature is even seen to decrease at $\sim 165 \text{ s}$ for the potentiostatic start-up of cell voltage (0.72 V) because the convective heat loss rate exceeds the total heat generation rate. Lowering the cell voltage from 0.72 to 0.55 V brings about an additional cell temperature rise of $\sim 3.0^{\circ}\text{C}$, the effect of which is comparable to lowering the heat convection coefficient from 40 to $0 \text{ W/m}^2/\text{K}$ (re-

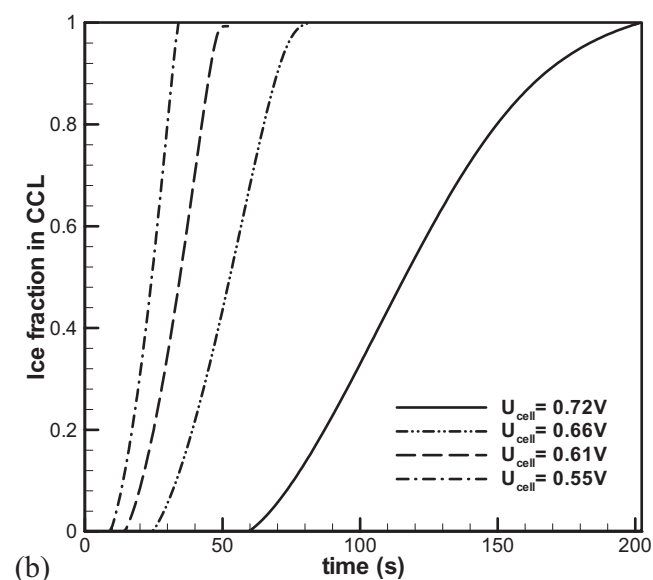
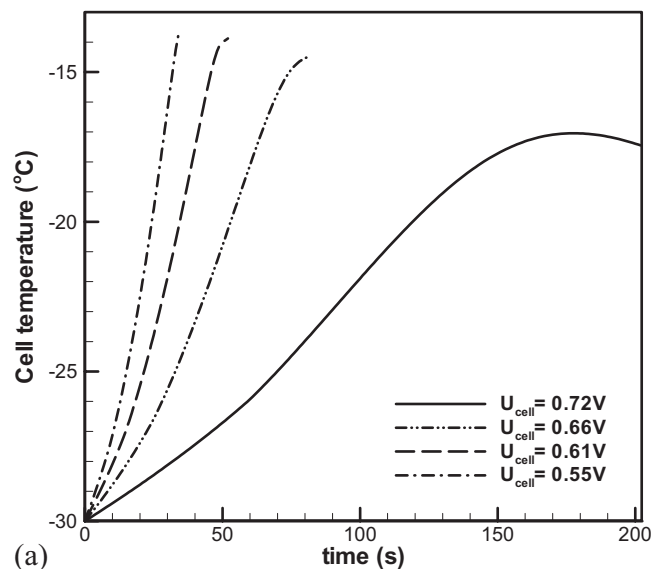


Figure 17. Evolution of (a) temperature and (b) ice fraction in the cathode CL during potentiostatic start-up from -30°C with various cell voltages.

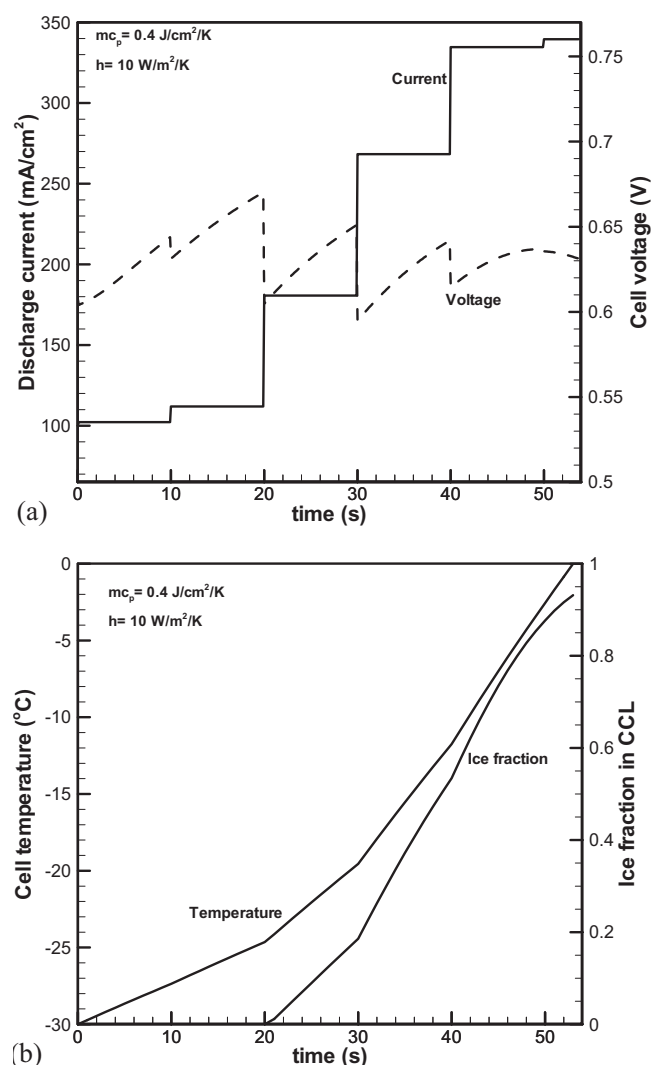


Figure 18. Evolution of (a) cell voltage and current density and (b) ice fraction in the cathode CL and cell temperature during a current-ramping start-up from -30°C .

fer to Fig. 11). As displayed in Fig. 17b, the ice fraction in the cathode CL reaches unity for all four cold-start operations, indicative of shutdown. The potentiostatic start-up of lower cell voltage shuts down faster due primarily to the faster water production rate.

Current-ramping start-up.—As potentiostatic start-up may not be directly applicable to fuel cell stacks, a current-ramping start-up is designed to exemplify application of the fundamental characteristics of potentiostatic start-up in practice. This start-up has a controlled current load; every 10 s the current load is increased to keep the resulting cell voltage roughly constant, thus creating a quasi-potentiostatic start-up. Evolution curves of current density and cell voltage, as well as cell temperature and ice fraction in the cathode CL, are displayed in Fig. 18. The cell voltage fluctuates mildly around 0.63 V, confirming the quasi-potentiostatic mode. Overall, the current density is low in the early stage of this start-up, offering time for hydration of the initially dry membrane; then, it quickly increases to create heat for cell temperature rise, and in the last stage of this start-up operation it remains almost unchanged to avoid excessive ice formation. It is seen from Fig. 18b that at ~ 53 s into

this start-up the cell temperature reaches 0°C while the ice fraction in cathode CL is still below unity, indicating a rapid self-start.

The present work clearly suggests that, as a special current-ramping profile, potentiostatic start-up is superior to the galvanostatic mode; however, the potentiostatic start-up may not be the best among all current-ramping profiles. Searching for an optimal current-ramping profile is of practical interest and should be pursued in future work.

Conclusions

Competition between heat generation and ice formation determines the fate of a cold start. Current-ramping start-up strategies take advantage of the improved membrane hydration and rising cell temperature during cold start, thereby permitting an aggressive increase in the operating current density with time and generating significantly more heat generation for rapid cell warmup. The rising temperature in turn leads to improved hydration of the membrane and reduction in ice formation in the cathode CL. Fundamentally, this new class of current ramping start-up protocols can be simulated and represented by the potentiostatic mode.

In this work, basic features of heat generation and ice formation are compared in potentiostatic and galvanostatic start-up. It is found that heat generation remains nearly constant or slightly decreases with time in galvanostatic operation, while it increases dramatically in potentiostatic start-up. As a result, the potentiostatic start-up from -20°C is successful, whereas the galvanostatic start-up from -20°C results in shutdown, under otherwise identical conditions. A prerequisite for potentiostatic start-up to be superior over galvanostatic start-up is that the membrane must be initially relatively dry. Other key factors controlling the effectiveness of potentiostatic start-up are cell thermal mass and convective heat loss from bipolar plates. Lowering the cell thermal mass can significantly improve the performance of potentiostatic start-up. Reducing convective heat loss from the end plates to the ambient is effective for long-duration start-up processes but less important for rapid start-up. Finally, numerical results predict that it is possible to achieve self start from -30°C in ~ 50 s under realistic conditions using either the potentiostatic or an equivalent current-ramping method.

Acknowledgments

We gratefully acknowledge Nissan Motor Co. Ltd. and NSF through grant no. 0609727 for financial support of this work.

The Pennsylvania State University assisted in meeting the publication costs of this article.

References

1. U.S. Department of Energy, Progress Report for Hydrogen, Fuel Cells, and Infrastructure Technologies Program, Appendix A (2002).
2. Y. Hishinuma, T. Chikashisa, F. Kagami, and T. Ogawa, *JSME Int. J., Ser. B*, **47**, 235 (2004).
3. M. Oszcipok, D. Riemann, U. Kronenwett, M. Kreideweis, and M. Zedda, *J. Power Sources*, **145**, 407 (2005).
4. L. Mao, K. Tajiri, S. Ge, X. G. Yang, and C. Y. Wang, Abstract 998, The Electrochemical Society Meeting Abstracts, Vol. 502, Los Angeles, CA, Oct. 16–21, 2005.
5. S. Ge and C. Y. Wang, *Electrochem. Solid-State Lett.*, **9**, A499 (2006).
6. L. Mao and C. Y. Wang, *J. Electrochem. Soc.*, **154**, B139 (2007).
7. K. Tajiri, Y. Tabuchi, and C. Y. Wang, *J. Electrochem. Soc.*, **154**, B147 (2007).
8. L. Mao, C. Y. Wang, and Y. Tabuchi, *J. Electrochem. Soc.*, **154**, B341 (2007).
9. K. Tajiri, Y. Tabuchi, F. Kagami, S. Takahashi, K. Yoshizawa, and C. Y. Wang, *J. Power Sources*, **165**, 279 (2007).
10. S. Ge and C. Y. Wang, *Electrochim. Acta*, **52**, 4825 (2007).
11. J. Hou, H. Yu, B. Yi, Y. Xiao, H. Wang, S. Sun, and P. Ming, *Electrochem. Solid-State Lett.*, **10**, B11 (2007).
12. E. L. Thompson, J. Jorne, and H. A. Gasteiger, *J. Electrochem. Soc.*, **154**, B1399 (2007).
13. S. Ge and C. Y. Wang, *J. Electrochem. Soc.*, **154**, B998 (2007).
14. J. Li, S. Lee, and J. Roberts, Paper 595 presented at The Electrochemical Society Meeting, Washington, DC, Oct. 7–12, 2007.
15. F. Jiang, W. Fang, and C. Y. Wang, *Electrochim. Acta*, **53**, 610 (2007).